Turbulence-airfoil interaction noise reduction using wavy leading edge: an experimental and numerical study

Cyril Polacsek, Vincent Clair, Gabriel Reboul, Hugues Deniau

大阪
inter.noise 2011
Osaka Japan September 4-7

Turbulence-airfoil interaction noise reduction using wavy leading edge: An experimental and numerical study

Cyril Polacsek[1], Vincent Clair[1], Gabriel Reboul[1], Hugues Deniau[2]

[1] ONERA (National Aerospace Research Establishment), Department of Numerical Simulations and Aeroacoustics, 92322 Châtillon Cedex, FRANCE

[2] CERFACS (European Centre for Research and Advanced Training in Scientific Computation), CFD Team, 31057 Toulouse Cedex 01, FRANCE

ABSTRACT

Passive treatments aiming at reducing turbofan broadband noise have been recently studied in the framework of European Project FLOCON. A concept based on a sinusoidal variation of the leading edge of a single airfoil expected to decrease interaction noise has been investigated by ONERA. Turbulence-airfoil interaction mechanism is achieved using a turbulence grid located upstream of a NACA airfoil tested in ISVR anechoic open wind tunnel. High noise reductions are obtained (3-4 dB) for all studied flow speeds. Experimental work is supplemented by numerical simulations using RANS/LES and CAA Euler-based approaches to predict the acoustic response of the wing. Isentropic turbulence is synthetically injected by means of a suited inflow boundary condition. Unsteady simulations are restricted to the baseline case (without treatment) and the present paper focuses on direct Euler methodology which provides reliable power spectrum density comparing to experiment. Effect of leading edge serrations on aerodynamics and noise is emphasized using Amiet thin airfoil theory, RANS solutions and available measurements.
Keywords: Turbulence interaction, Turbofan Noise, Computational Aeroacoustics.

1. INTRODUCTION

Turbulent wakes generated by turbofan blades and interacting with the OGV are known to be mainly contributing to broadband noise emission of aero engines at approach conditions. Passive treatments aiming at reducing fan broadband noise have been recently studied in the framework of European Project FLOCON [1-3]. A concept based on a tri-dimensional sinusoidal modification of the LE (leading edge) of a single airfoil has been investigated by ONERA [3]. Turbulence-airfoil interaction mechanism is achieved using turbulence grids located upstream of a NACA 651210 airfoil in the ISVR anechoic open wind tunnel [4]. Three airfoil sets with different values for wavelength and wave amplitude have been tested and compared to the reference wing response. A circular microphone antenna located at about three spans from the airfoil provides acoustic spectra and OASPL (Overall Sound Pressure Level) directivity. High noise reductions are measured (up to 6 dB) for a wide frequency range, leading to at least 3 dB attenuation of acoustic power. Moreover, aerodynamic performances are shown to be slightly increased by the treatment that tends to reduce the turbulent wake intensity beyond the TE (trailing edge), the (spanwise averaged) static pressure distribution being roughly unchanged. Experimental work is supplemented by CAA (Computational Aero-Acoustics) aiming to simulate the aerodynamic and acoustic responses. Present computations are devoted to the baseline case (without treatment), since treated case is still underway. First predictions based on analytical Amiet formulation [5] were found to be close to the measurements,

[1] cyril.polacsek@onera.fr

but extension of the theory to varying edges seems only feasible for basic topologies requiring unpractical simplifications [6]. In order to try to take into account true airfoil geometry and realistic mean flow, numerical approach is certainly the only issue. Methodologies based on hybrid RANS/LES and direct Euler computations have been investigated and presented in [3,7]. In both cases, HIT (homogeneous isentropic turbulence) is synthetically injected by means of divergence-free velocity disturbance field distributed over Fourier-modes with random phases. LES is chained to a FWH integral to get the acoustic far-field.

In the present paper, more analyzes of the effect of wavy-edge are proposed with the help of thin airfoil theory, RANS solutions, and available wind tunnel measurements. Numerical predictions (spectra and directivities) are restricted here to the direct Euler approach for which preliminary 2D computations have been extended to 3D. Because the 3D simulations are not fully converged at this time, only the 2D approach is presented including an efficient correction applied for simulating tridimensional effects. Compared to previous shorter paper [3], more details are given about aerodynamic behavior, serration effects, and CAA features. Hence, ability of numerical approach in view of quantifying the acoustic efficiency of leading-edge serrations is clearly addressed.

2. WAVY LEADING EDGE CONCEPT DESCRIPTION

Wavy edge treatment has been recently studied by Hansen et al. [8] for aerodynamic performance purpose, following previous investigations on aerodynamic effects of whale flipper leading-edge rounded protuberances (so-called tubercles) [9]. It was shown that tubercles act as vortex generators which could increase the lift and delay the stall. This concept has been also applied to rotor blades in order to try to reduce the tone noise caused by blade vortex interactions [10].

Wavy-edge concept is illustrated in Fig. 1, showing a 3D CAD view with two main adjustment parameters (wavelength, λ and amplitude, A) and a picture of one of the manufactured ONERA wings. The present study is devoted to acoustic performance with respect to turbulence-airfoil interaction (broadband) noise reduction, assuming that acoustic sources are located in the leading edge region. Sinusoidal variations of the chord length and lean angle are expected to introduce some spanwise correlation loss and to modify the response to the impinging gusts (turning parallel cut-on modes to oblique cut-off modes). These effects will be more discussed in section 4.

Three sets of wings have been manufactured and tested :

- λ = 6 mm and A = 10 mm (referred as 1S)
- λ = 10 mm and A = 10 mm (referred as 2S)
- λ = 10 mm and A = 15 mm (referred as 3S)

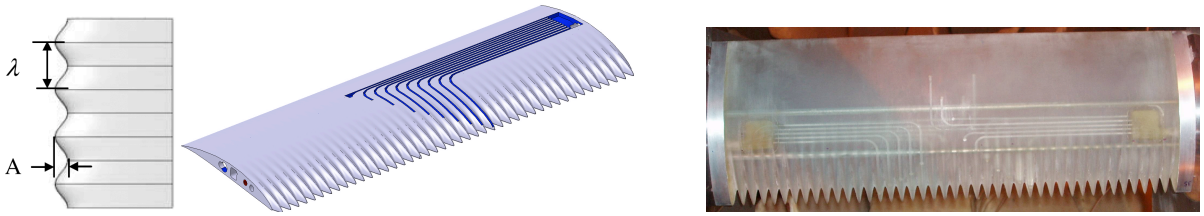

Figure 1. FLOCON wing design: CAD drawing (left) and manufactured wing (right)

3. TEST SET-UP, NOISE REDUCTION AND AERODYNAMIC PERFORMANCES

ONERA wings have been tested in the ISVR anechoic wind tunnel [2,4] and compared to the baseline case at several flow speeds (U_0 = 20, 40, 60 m/s) and for different angles of attack (α = 0°, 5°, 10°, 15°). Experimental set-up is presented in Fig. 2, showing the circular antenna (located at 1.2 m from the airfoil) used to get the far-field PSD (Power Spectral Density) and directivities. When possible, in order to trigger a turbulent boundary layer a tripping band made of rough sand paper is attached on surface of the airfoil at 10% of the chord. A square-rods turbulence grid located inside the nozzle near the outlet provides selected HIT characteristics (validated by comparison to usual Von-Karman spectrum) upstream of the airfoil, with a turbulence intensity, T_I = 2.5 %, and an integral length scale, Λ = 6 mm. Hence, interaction noise (measured with the grid) is found to be

largely dominant compared to the airfoil self-noise, as shown in Fig. 3 for two flow speeds. PSD measured at 90° for the three treatments are compared to the baseline in Fig. 4 (α = 0°), showing high noise reduction for a wide frequency range, more particularly at low speed. Best performance is obtained with treatment 3S. Fig. 5 summarizes the noise level reductions obtained with treatment 3S, by integrating the spectra in the range [300 Hz -20 kHz]. It shows that good performance is reached for all angles of attack values up to $\alpha = 15°$. Fig. 6 (left) compares PSD between wing 3S and baseline (0S), highlighting large noise reductions in the mid-frequency range (about 6 dB at 3 kHz). OASPL directivity related to microphone antenna and calculated by integrating the spectra from 1 kHz is shown in Fig. 6 (right). Acoustic performance appear to be slightly reduced in the front arc (gain of 3 dB) compared to the rear one (gain of 5 dB).

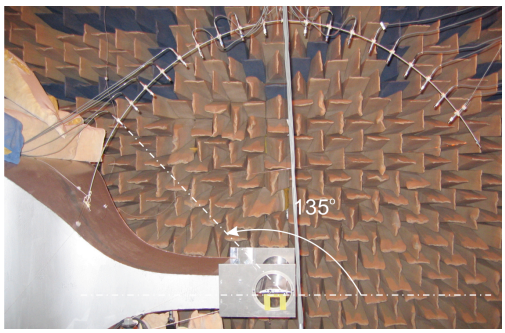

Figure 2. Experimental set-up in ISVR rig

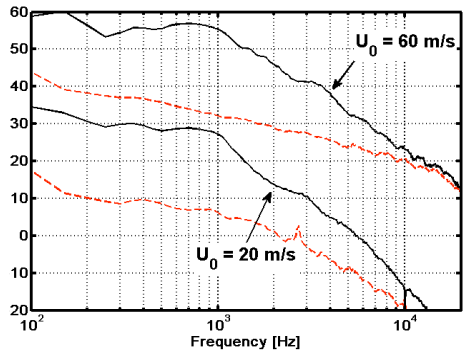

Figure 3. Interaction (black) and self (red) noise spectra

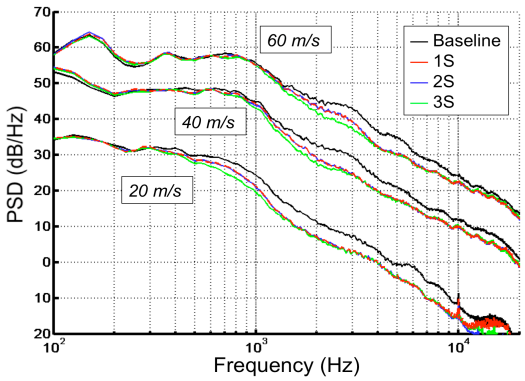

Figure 4. Baseline and ONERA wing spectra (90°)

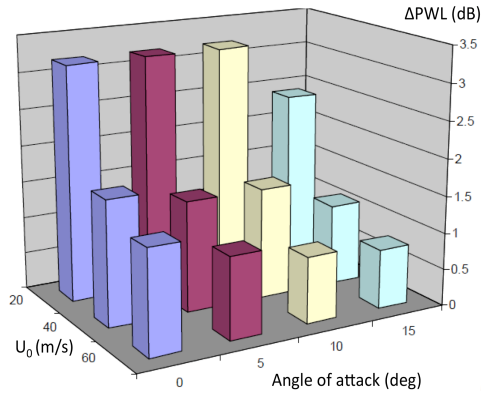

Figure 5. PWL reductions (dB) using 3S wing

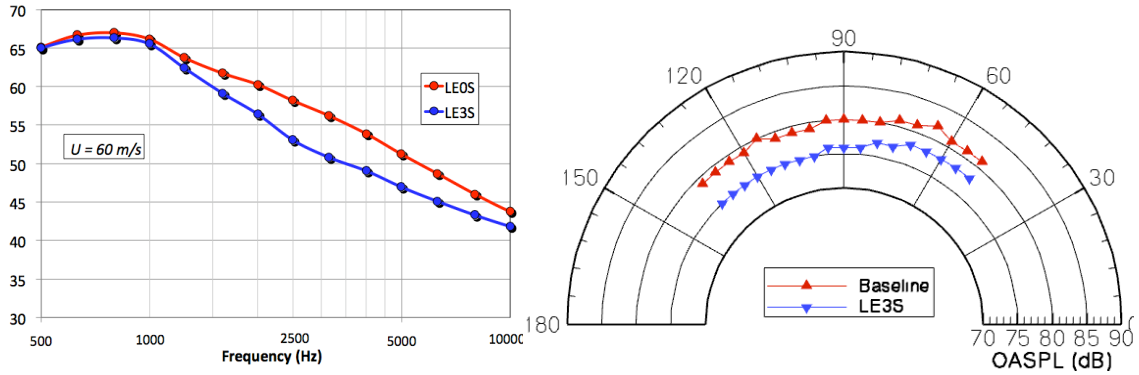

Figure 6. Baseline-3S comparisons of PWL (left) and OASPL directivities (right) at higher speed (60 m/s)

Aerodynamic behavior has been also investigated in order to check the effect of leading edge serrations on aerodynamic performances. RANS computations using ONERA code *elsA* have been performed by Cerfacs using different strategies [7]. Figure 7 displays C_p distributions issued from RANS and measurements at mean exit flow U_0 = 60 m/s and for two angle of attack (α = 0° and

$\alpha = 10°$). As shown by Moreau et al. [11], the nozzle exit flow has to be fully included in the RANS simulation to match open jet wind tunnel conditions. As discussed in [7], URANS time-averaged computations have to be performed then to ensure the convergence of the solution. As shown in Fig. 7, a very nice agreement between predictions and tripped airfoil measurements is obtained when jet flow is taken into account.

Comparisons of C_p distributions measured at ISVR on baseline 0S (no serrations, no trip) and 2S ONERA wing (using sensors located on the top of the waves) are shown in Fig. 8 for the same angles of attack. No trip was used is that case, because it was unpractical to attach the tripping band along the waves. Noticeable differences are visible at the leading edge region. Away, distributions are almost similar. Consequently, integration of the C_p for serrated edge case lead to an important increase of the lift. Similar trends have been obtained for other configurations. However, this positive effect in terms of aerodynamic performance should be pondered as sensors are located on top wave, and as bottom wave measurements would probably not display the same behavior.

To check this point RANS computations have been performed on 2S wing assuming a uniform mean flow (jet flow discarded), which is reasonable for estimating the relative effect of serrations. A close-up view of CFD wavy-edge skin mesh is shown in Fig. 9, left, and computed C_p at three spanwise positions (top, mid, and bottom) are plotted in Fig. 9, right. Away from leading edge region, C_p distributions are found to be almost identical, according to the measurements. Moreover, the bottom wave solution is quite similar to the baseline (uniform flow) shown in Fig. 7 (left), and the relative deviation highlighted in Fig. 9 right between bottom wave and top wave distributions are in a fairly good agreement with experimental trends observed in Fig. 8 left between baseline and 2S (top wave). These are convincible results with respect to wavy-edge aerodynamic performances. Finally, these investigations are completed by iso-velocity contour map analyzes issued from 2D RANS (baseline case) and 3D RANS (wavy-edge case) computations presented in Fig. 10 (same scales for all plots). The baseline solution roughly matches the wavy-edge solution averaged over the span.

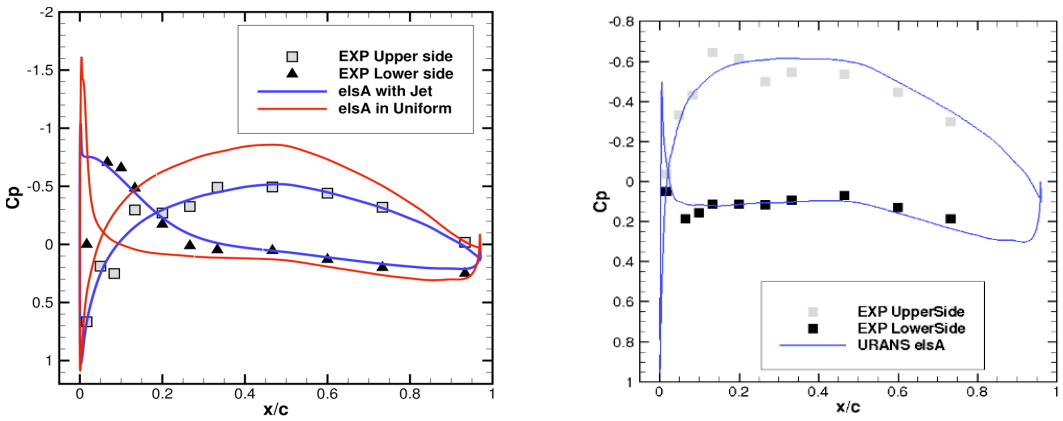

Figure 7. C_p distributions issued from RANS and measurements at $\alpha = 0°$ (left) and $\alpha = 10°$ (right)

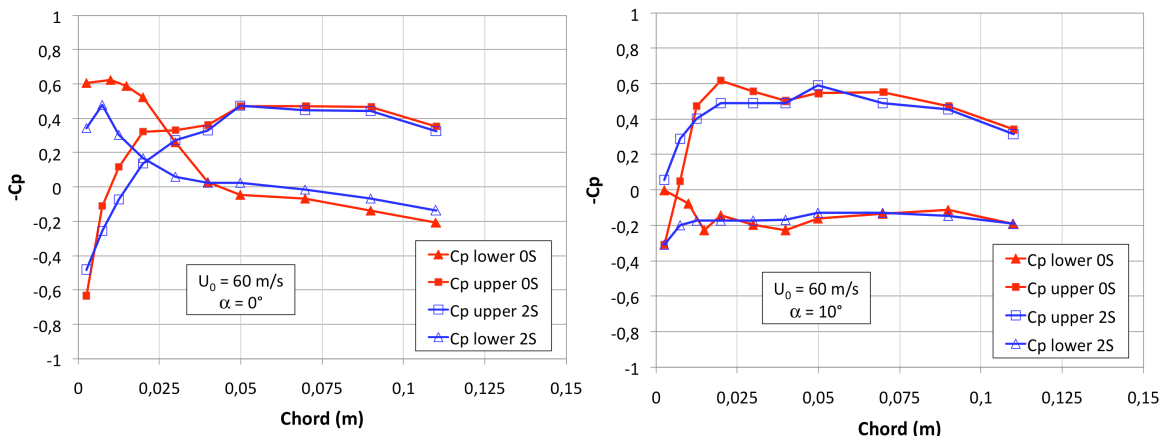

Figure 8. C_p distributions for baseline and ONERA 2S wing measured at $\alpha = 0°$ (left) and $\alpha = 10°$ (right)

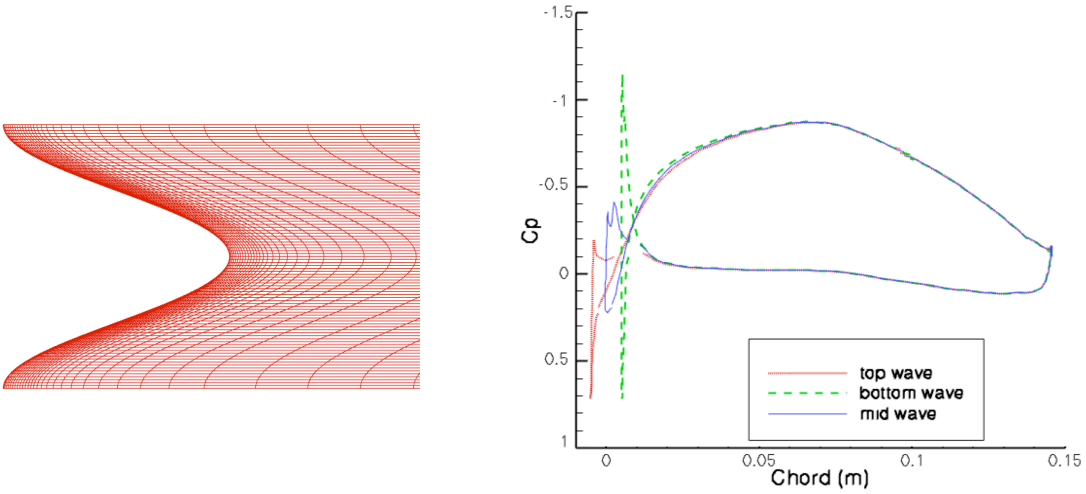

Figure 9. 3D RANS wavy-edge mesh (left) and computed C_p distributions (U_0 = 60 m/s, α = 0°)

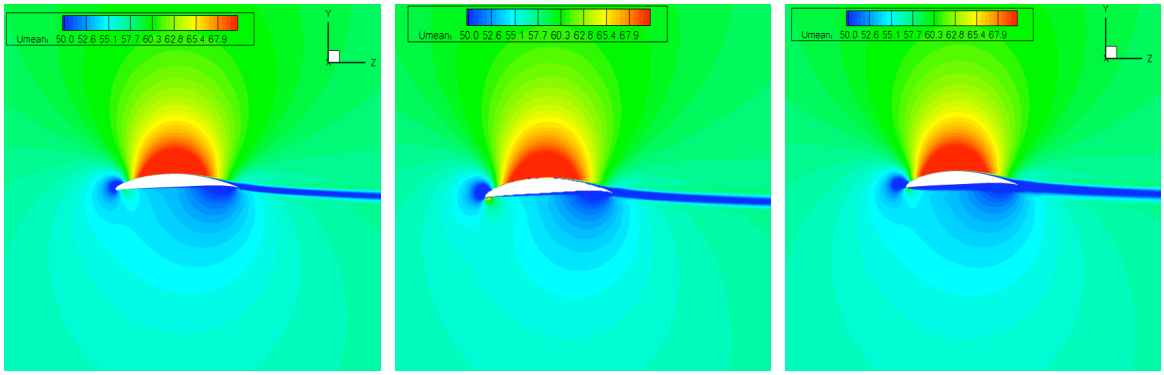

Figure 10. Spanwise cuts of RANS mean flow velocity field around 2S and baseline wings: 2S top wave (left), baseline (middle), and 2S bottom wave (right)

4. ACOUSTIC PREDICTIONS FROM ANALYTICAL AND NUMERICAL METHODS

4.1 Integral formulations and Amiet-based predictions

Following Amiet theory [5], the problem of turbulence-airfoil interaction can be modelized as a summation of harmonic gusts impinging a flat plate as sketched in Figure 11. The gusts are time and space Fourier-modes in the chordwise and spanwise directions. K_ζ and K_η are the aerodynamic wave numbers in the local coordinate system (ζ,η,ξ).

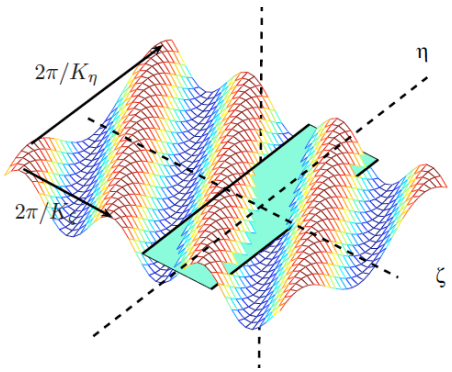

Figure 11. Sketch of gust-airfoil problem

The aerodynamic response of the airfoil, $g\left(\zeta,K_\varsigma,K_\eta\right)$, is calculated by solving a convected wave equation written for the potential of a velocity perturbation (satisfying this equation). The wall-pressure jump, Δp, then writes:

$$\Delta p\left(\zeta,\eta,t\right)=2\pi\rho_0 U_c\int_{-\infty}^{+\infty}\int_{-\infty}^{+\infty}\hat{\hat{u}}_\xi\left(K_\varsigma,K_\eta\right)g\left(\zeta,K_\varsigma,K_\eta\right)e^{i\left(K_\zeta U_\zeta t-K_\eta\eta\right)}dK_\zeta dK_\eta \tag{1}$$

$\hat{\hat{u}}_\xi$ denotes the double space-Fourier transformation of incoming velocity fluctuation normal to the plate, and U_ζ is the chordwise velocity (taken equal to the convection velocity U_c) related to the convection wave number using Taylor assumption (frozen turbulence): $K_\varsigma=K_c=\dfrac{\omega}{U_c}$. The radiated acoustic field is obtained by using Curle's formulation:

$$\hat{p}\left(\vec{X},\omega\right)=\int_S\hat{p}\left(\vec{Y},\omega\right)n_i\frac{\partial G_\omega\left(\vec{X},\vec{Y}\right)}{\partial y_i}dS \tag{2}$$

where ^ denotes the time-Fourier transform, $\vec{X}$ and $\vec{Y}$ are the observer and source coordinates, respectively, and G_ω denotes the free-space time-Fourier transformed Green's function. The PSD of acoustic pressure, $S_{pp}\left(\vec{X},\omega\right)$, is estimated by injecting Eq. (1) in Eq. (2) and by performing the integral of the cross-conjugate product over spatial directions and spanwise wave-number. Far-field assumption (KR >>1) allows us to make some mathematical simplifications so that a rather concise expression is obtained:

$$S_{pp}\left(\vec{X},\omega\right)=\left(\frac{kz\rho_0 b}{S_0^2}\right)^2 U_c d\pi\int_{-\infty}^{+\infty}\left[\frac{\sin^2\left(d\left(\dfrac{ky}{S_0}-K_\eta\right)\right)}{\pi d\left(\dfrac{ky}{S_0}-K_\eta\right)^2}\right]\left|\mathcal{L}\left(x,K_c,K_\eta\right)\right|^2\phi_{\xi\xi}\left(K_c,K_\eta\right)dK_\eta \tag{3}$$

$\mathcal{L}$ is the aeroacoustic transfer function given by Amiet. The wave-number PSD of normal velocity fluctuation, $\phi_{\xi\xi}\left(K_c,K_\eta\right)$, can be estimated by means of a 2D Von-Karman turbulence energy spectrum model fitted by experimental input data (Λ and T_I). In the case of parallel gusts (which are known to be mainly responsible of radiated interaction noise), $\phi_{\xi\xi}\left(K_c,0\right)$ can be directly related to the spanwise correlation lengthscale, ℓ_y, and to the standard frequency spectrum of u_ξ:

$$\phi_{\xi\xi}\left(K_c,0\right)=\frac{U_c}{\pi}\ell_y\left(\omega\right)\phi_{\xi\xi}\left(\omega\right) \tag{4}$$

Predicted PSD at 90° and OASPL directivities are compared to the ISVR measurements in Figs. 12 and 13, respectively. A fairly good agreement is obtained, particularly at the lowest speed. An under-estimation of the spectrum slope can be noticed at higher speeds. This confirms that Amiet model is able to assess THI-airfoil noise, but extension of this theory to account for varying edges does not seem feasible without drastic simplifications [6]. This is the reason why a numerical approach has been proposed and is presented in section 4.3. However, thin airfoil theory can be used to overcome basic understanding and to suggest a raw design of the serrations, as discussed in the next paragraph.

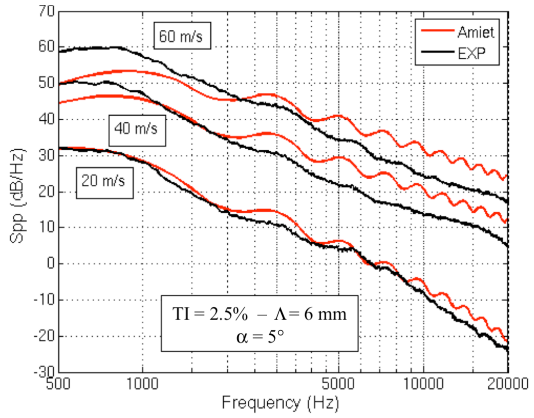

Figure 12. Predicted and measured PSD at 90°

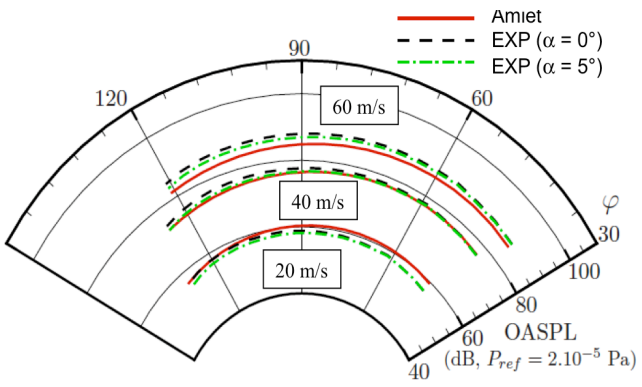

Figure 13. Predicted and measured OASPL directivities

4.2 Serration design

Helping from ISVR turbulence grid characteristics and thin airfoil theory, basic mechanisms that might be considered for serration design (A and λ parameters described in section 2) are discussed here. Firstly, the wavelength can be adjusted with respect to the spanwise correlation lengthscale ℓ_y involved in Eq. (4). This scale, function of frequency, can be expressed from turbulence lengthscale and convection wave number (assuming Von-Karman spectrum model). It is plotted in Fig. 14, for two convection speeds. De-correlation effects might be noticeable if chord variation between two point-sources is large enough and if these sources are fully correlated (distance between them lower than ℓ_y). We can assume that these effects are optimal when λ/2 is roughly equal to the maximum size of ℓ_y (which is mostly equal to Λ = 6 mm). The span being equal to 450 mm, λ is rounded to 10 mm (wings 2S and 3S) so that it can be splitted into N_{wave} motifs (N_{wave} = 45). The wing 1S was designed using the mean value of ℓ_y (about 3 mm) leading to λ = 6 mm (N_{wave} = 75).

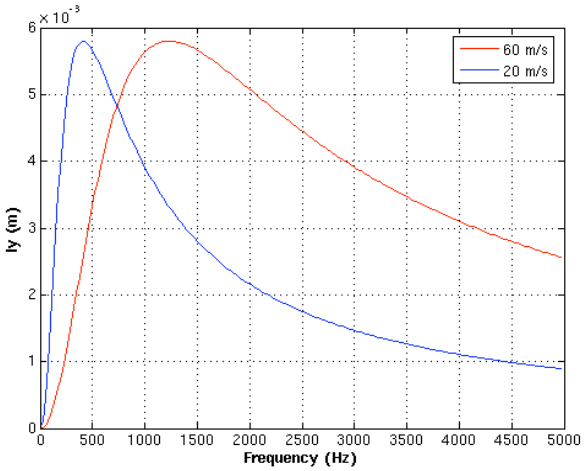

Figure 14. Spanwise correlation lengthscale deduced from ISVR turbulence grid characteristics

Secondly, the amplitude has to be set. It seems reasonable to think that A should be larger as possible to expect higher effects with respect to local chord and lean angle value. However, the amplitude range has to be limited by aerodynamic constraints, since modifications of the stream flow are expected to increase with A, whereas performance and stability have to be preserved. Because CFD calculations were expected to be launched after the airfoil treatment design (to be implemented and manufactured at the beginning of FLOCON project), it was decided to limit the amplitude value to 10% of the chord length (A ≤ 15 mm). The effect of lean angle on acoustic response of the airfoil can be assessed from Amiet theory extended to the case of a chord varying in the spanwise direction, and by introducing the leading edge equation in the convected wave equation with suited variable transformations, as originally proposed by Rozemberg (ONERA non-published work). Simplifying

the sinusoidal wave to a triangular wave (as sketched in Fig. 15), the usual dispersion relation valid for a straight leading edge can be generalized as:

$$k^2 = \left(\frac{\bar{K}_\xi M}{\beta^2} \right)^2 - \left(\bar{K}_\xi M^2 \tan\gamma + \frac{\bar{K}_\eta M^2}{\beta^2} \right) \tag{5}$$

The symbol "–" denotes the normalization by the half-chord, and γ is the lean angle (Fig. 15) given by $\tan\gamma = \frac{2A}{\lambda}$. Eq. (5) turns to Amiet dispersion relation by setting A = 0. Following Graham rules, the sign of k^2 determinates the nature of the gusts that are cut-on (cut-off) if $k^2 > 0$ ($k^2 < 0$). A physical interpretation of this result is presented in Fig. 16, visualizing the spectral filtering of oblique gusts in the plane (K_ξ, K_η). The cut-on modes (supercritical gusts) are highlighted by conical surfaces that are deviating from the chordwise direction as the lean angle is increasing. The value $\gamma = 71.6°$ corresponds to the S3 wing with triangular wave assumption. Practically, this value is larger since the tangent to the sinus at $\xi = 0$ is more inclined than for the triangle case (see Fig. 15). Hence, parallel gusts $(K_\xi, 0)$ and neighboring ones (K_η small) being the most energetic modes in terms of acoustic radiation, it is clearly observed that for lean angles getting close to 90° (A getting high) these modes tend to be filtered so that noise reduction may be expected.

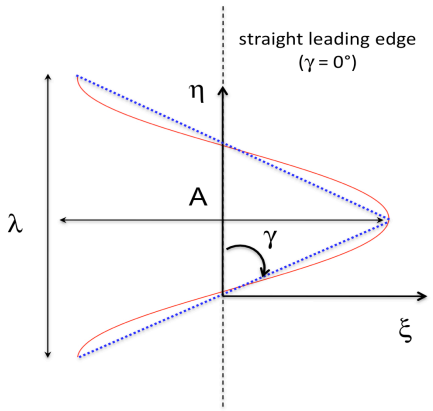

Figure 15. Sketch of triangular wave geometry

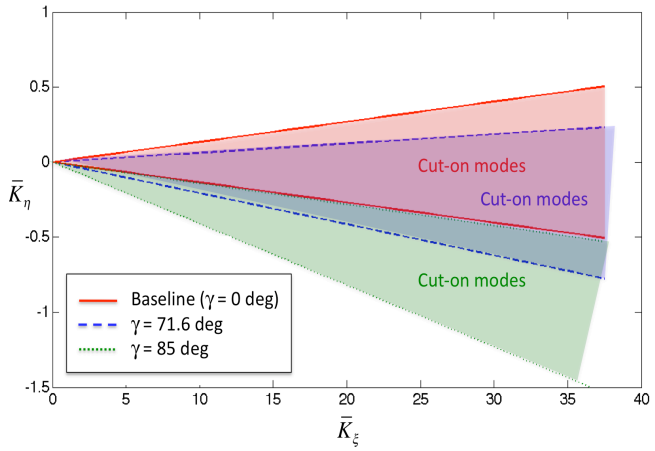

Figure 16. Spatial filtering of oblique gusts

4.3 Direct Euler computations

In order to simulate the leading edge treatment effects on acoustics, a numerical methodology using ONERA code *sAbrinA* [12,13] has been investigated. The code solves the non-linear Euler disturbances in the time domain using a high-order dispersion preserving scheme. First computations are focused on the baseline case for which our CAA was restricted to 2D, for simplicity. 3D computations are underway (not converged yet) and should confirm the 2D results discussed here (without having to apply 2D to 3D corrections used in this section). Of course, 3D will be also mandatory for simulating the serrated case. Incoming turbulent flow is generated by means of harmonic velocity perturbations (following Amiet formalism) using a synthetic turbulence model [14,15], and injected through a suited inflow BC (boundary condition) proposed by Tam [16]. Outflow BC are based on Tam radiation condition assuming spherical (or cylindrical) waves with point-source located at the center of the airfoil. These BC are required for injecting and convecting acoustic and hydrodynamic modes without creating artificial noise. As done in [14], only parallel gusts (K_ζ in Fig. 7) are imposed, with amplitudes adjusted using 1D Von-Karman energy spectrum (since computations are 2D) as specified in [15]. It is obtained by integrating the 2D spectrum of Eq. (4) along spanwise wave numbers.

The turbulent transverse velocity fluctuation u_y (ξ direction in Fig. 11) injected at the inflow boundary then writes:

$$u_y(x,t) = \sum_{n=1}^{N_{max}} \sqrt{\phi_{\xi\xi}(k_{c,n})\Delta k_c}\,\cos\left[k_{c,n}(x - U_c t) + \varphi_n\right],\quad \varphi_n = random\{0, 2\pi\} \qquad (6)$$

Wave number spacing (Δk) is equal to $2\pi/X_L$ where X_L is the axial length (0.4 m) of CAA domain. A random phase (φ_n) is used to reproduce a stochastic process. Realistic mean flow (U_c = 60 m/s) from nozzle exit is provided by a 2D RANS computation performed with *elsA* [6]. This flow is then interpolated of the CAA grid adapted for acoustics to satisfy 10-points per (smallest) wavelength considered here (f_{max} = 5 kHz) and a local CFL lower than unity. A view of CAA multi-bloc grid (1 point over 4) is shown in Fig. 17, left. To avoid numerical difficulties when injected velocity disturbances are crossing the shear layer of nozzle exit flow, interpolated RANS mean flow is also modified to mimic flight conditions with homogeneous uniform mean flow. This "adapted" mean flow for which initial RANS solution in the vicinity of the airfoil is fully preserved is plotted in Fig. 17 (right). An iso-contour snapshot of turbulent velocity fluctuations impinging the airfoil is shown in Fig. 18 (left) and acoustic response in terms of pressure iso-contour snapshot is shown in Fig. 18 (right). Expected dipolar behavior is correctly assessed by the 2D simulation. Vortical waves convected along the airfoil pressure side and beyond the trailing edge are clearly visible too.

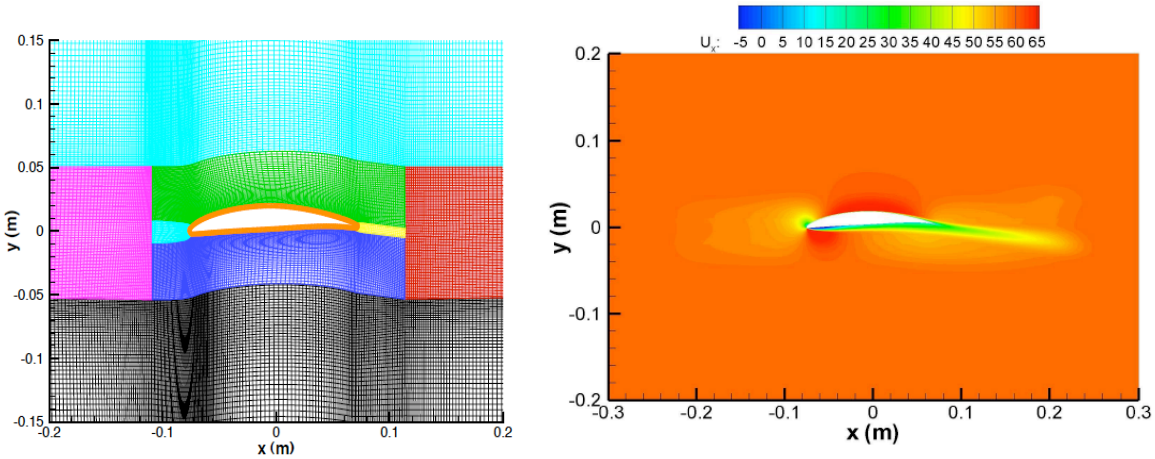

Figure 17. 2D CAA multi-bloc grid around airfoil (left) and RANS interpolated mean flow (right)

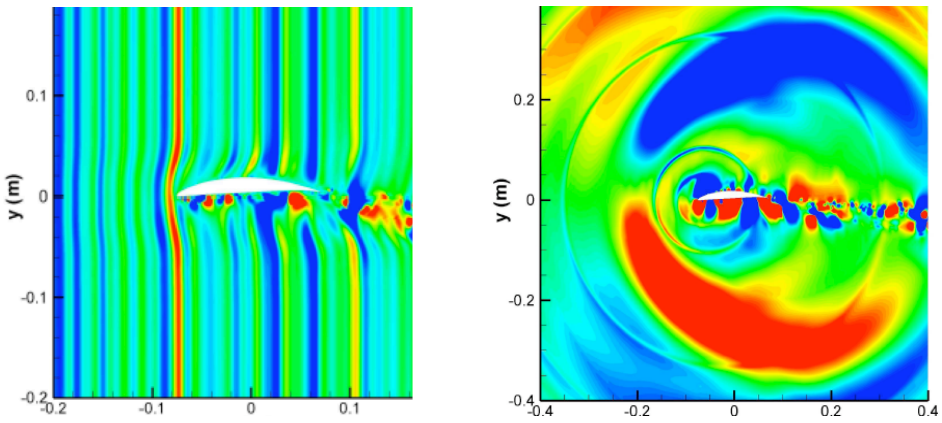

Figure 18. Synthetic turbulent velocity field (left) and direct acoustic pressure radiation (right)

Computed PSD at 90° for an observer at 0.35 m from the centre of the airfoil is presented in Fig. 19 (left, blue curve) and compared to the same simulation assuming a fully uniform flow (green curve with dots), and to the analytical solution issued from Amiet theory (dotted line). The agreement between CAA (uniform flow) and Amiet predictions is quite good, whereas a higher attenuation slope can be noticed for the CAA solution with a RANS mean flow. This could explain

the slope deviation observed in Fig. 12 and discussed in Section 4.1. Similar comparisons on OASPL directivities are proposed in Fig. 19 (right), showing that the three predictions are almost identical in the front arc and that differences with Amiet solution are more marked in the upside rear arc. Upside/downside dissymmetry due to the fact that the airfoil is not symmetrical (whereas it is assumed to be in Amiet theory) is clearly highlighted by the CAA.

In order to compare the 2D simulations with the ISVR measurements, a simple correction proposed by Ewert et al. [17] is applied to the PSD. It writes:

$$S_{pp}^{3D}(\omega) = S_{pp}^{2D}(\omega) \times \frac{k\ell_y(\omega)L}{2\pi R_{obs}} \tag{7}$$

ℓ_y is the spanwise correlation length (scaled from L and Von-Karman model), and L is the airfoil span. This correction was found to be very accurate when applied to Amiet 2D and 3D direct solutions. PSD so obtained at 1.2 m (90°) microphone is compared to the measurements in Fig. 20. Smoothed CAA curve (pink curve) is found to be very close to the experiment (red curve) in the range [500 Hz – 5 kHz], making our CAA methodology rather promising.

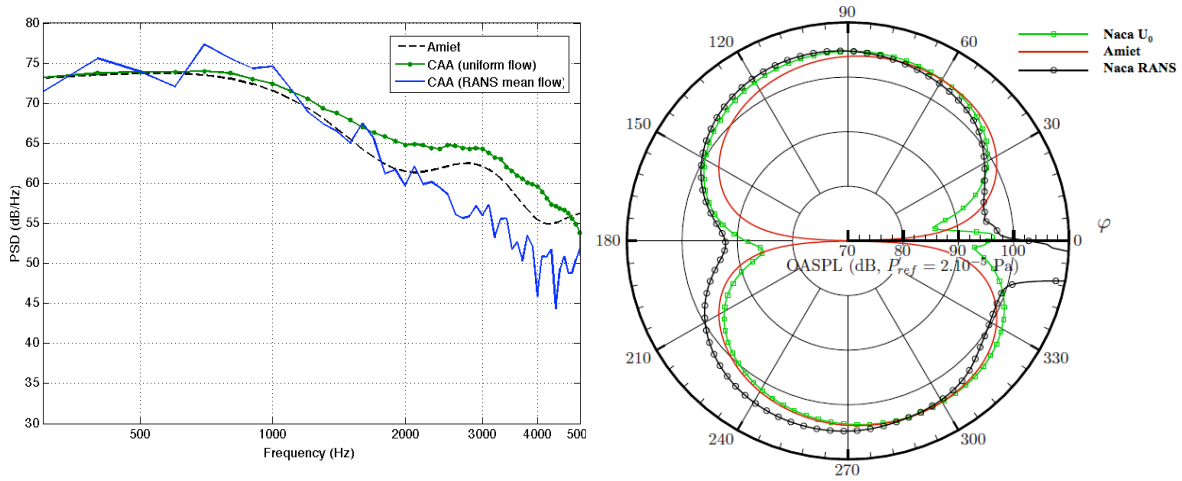

Figure 19. Predicted 2D spectra (dB/Hz) and OASPL (dB) directivities

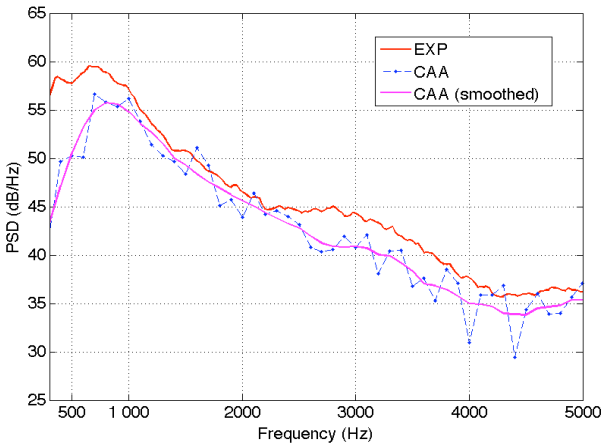

Figure 20. Predicted and measured 3D spectra (dB/Hz)

5. CONCLUSIONS

A wavy leading edge treatment consisting in tridimensional sinusoidal serrations devoted to turbulence-airfoil interaction noise reduction has been applied to an isolated NACA airfoil impacted by a turbulent flow. Experimental data issued from wind tunnel tests have shown significant

broadband noise reductions for a wide frequency range, and for almost all configurations. Aerodynamic performance suggested by recent studies has been partly confirmed too. This makes this concept very attractive for quieter turbofans as it could be easily implemented on the stator vanes. Different methodologies aiming at simulating the acoustic efficiency of the treatment have been proposed. First predictions are performed on the baseline case (no treatment). Analytical calculations based on Amiet theory were found to be reasonably confident for estimating the interaction noise emitted by a standard airfoil, and were used to give some basic understanding of the wavy edge effects. Since full extension of Amiet theory to varying edges is not feasible, numerical strategies have been investigated. A hybrid approach based on affordable LES was presented in [7]. Present paper only focused on direct Euler computations (neglecting viscosity effects), in which a synthetic (incoming) turbulence was assessed by means of prescribed velocity perturbations injected through a suited inflow boundary condition (as done in [7]). This CAA method applied in 2D was found to be very promising, providing PSD in a quite good agreement with the measurements.

Next step will be to extend these CAA simulations to 3D in order to numerically estimate the efficiency of the serrations and to compare with the acoustic performance measured during the tests.

ACKNOWLEDGEMENTS

This work was supported by European Commission (FLOCON).

REFERENCES

[1] L. Enghardt, The EU FP7 Research Project FLOCON – Objectives and First Results, *Internoise 2010*, Lisbon, Portugal, June (2010).

[2] M. Gruber, P. Joseph, P. and T. P. Chong, Experimental Investigation of Airfoil Self Noise and Turbulent Wake Reduction by the Use of Trailing Edge Serrations, *16th AIAA/CEAS Conference*, Paper 2010-3803, Stockholm, Sweden, June (2010).

[3] C. Polacsek, G. Reboul, V. Clair, T. Le Garrec, G. Dufour, H. Deniau, Turbulence-Airfoil Interaction Noise Reduction Using Wavy Leading Edge: An Experimental and Numerical Study, *ICSV18*, Rio, Brazil, July (2011).

[4] T. P. Chong, P. F. Joseph, P.O.A.L. Davies, Design and Performances of an Open Jet Wind Tunnel for Aero-Acoustic Measurement, *Applied Acoustics* **70**, 605-614 (2009).

[5] R. K. Amiet, Acoustic Radiation from an Airfoil in a Turbulent Stream, *J. Sound Vibration* **41**, 407–420 (1975).

[6] M. Roger, A. Carazo, Blade-Geometry Considerations in Analytical Gust-Airfoil Interaction Noise Models, *16th AIAA/CEAS Conference*, Paper 2010-3799, Stockholm, Sweden, June (2010).

[7] G. Dufour, H. Deniau, J. F. Boussuge, C. Polacsek, S. Moreau, Affordable Compressible LES of Airfoil-Turbulence Interaction in a Free Jet, *17th AIAA/CEAS Conference*, Portland, USA (2011).

[8] K. L. Hansen, R. M. Kelso, B. B. Dally, Performance Variations of Leading-Edge Tubercles for Distinct Airfoil Profiles, *AIAA Journal* **49**, (2011).

[9] D. S. Miklosovic, M. M. Murray, L. E. Howle and F. E. Fish, Leading-edge Tubercles Delay Stall on Humpback Whale (Megaptera novaeangliae) Flippers, *Physics of Fluids* **16**, (2004).

[10] J. Feinerman, S. Koushik, F.H. Schmitz, Effect of Leading-Edge Serrations oh Helicopter Blade-Vortex Interaction Noise, *AHS 67th Annual Forum*, Virginia Beach, VA, May (2011).

[11] S. Moreau, M. Henner, G. Iaccarino, and M. Wang, Analysis of Flow Conditions in Freejet Experiments for Studying Airfoil Self-Noise, *AIAA Journal*, 41(10), 2003.

[12] S. Redonnet, E. Manoha, P. Sagaut, Numerical Simulation of Propagation of Small Perturbations Interacting with Flows and Solid Bodies, *7th AIAA/CEAS Conference*, Paper 2001-222 (2001).

[13] G. Reboul, C. Polacsek, Towards Numerical Simulation of Fan Broadband Noise Aft Radiation From Aero-engines, *AIAA Journal* **48**, 2038-2048 (2010).

[14] J. Casper, F. Farassat, A new time domain formulation for broadband noise predictions, *International Journal of Aeroacoustics*, **1**, 207–240 (2002).

[15] M. Dieste, G. Gabard, Synthetic Turbulence Applied to Broadband Interaction Noise, *15th AIAA/CEAS Conference* , 2009-3267 (2009).

[16] C. K. W Tam, Advances in Numerical Boundary Conditions for Computational Aeroacoustics, *J. Computational Acoustics* **6**, 377-402 (1998).

[17] R. Ewert, C. Appel, J. Dierke, M. Herr, RANS/CAA Based Prediction of NACA 0012 Broadband Trailing Edge Noise and Experimental Validation, *15th AIAA/CEAS Conference*, 2009-3269 (2009).